Stiffness Analysis of Underactuated Fingers and Its Application to Proprioceptive Tactile Sensing

Bruno Belzile and Lionel Birglen, *Member, IEEE*

***Abstract*—Underactuation has become, in recent years, more and more prevalent in robotic fingers since it provides the latter with the ability to mechanically adapt to the shape of the objects seized. To improve the usually simplistic control schemes of these fingers, and possibly to provide force feedback or control, tactile sensors are typically used. However, another promising avenue, as presented in this paper, is rather to use information provided by proprioceptive (i.e., internal) sensors. Most interestingly, this can be done using only the torque and position sensors typically found attached to the actuator(s) of these fingers. Because a relationship exists between the stiffness of an underactuated finger as seen from its actuator and the contact locations on its phalanges, it is possible to estimate one from the other. In this paper, a proprioceptive tactile sensing algorithm based on this technique is presented. It is concluded that within certain theoretical and practical limits, it is possible to extract tactile data from a self-adaptive finger, namely position and magnitude of the contact forces, without actually using any physical tactile sensors.**

***Index Terms*—Grasping, kinetostatics, proprioception, stiffness analysis, tactile sensing.**

I. Introduction

GRASPING has been a most common application of robotic systems for many decades. Robots capable of seizing objects have been used for many tasks ranging from assembly lines, space systems, to medical devices. While many commercial grippers, hands, and prototypes of these have been built based on fully actuated designs where each degree of freedom is associated to a specific actuator, underactuated mechanisms have become a strong challenger to the status quo in recent years. Underactuated, a.k.a. self-adaptive, fingers, and hands rely on fewer actuators than the number of their degrees of freedom and are now well known for their capability to mechanically envelop objects of various shapes, making them particularly well suited for grasping tasks [1]. While underactuated mechanisms have existed sometimes for centuries, their use in robotics and grasping has grown significantly since the first widely known prototype, namely the *Soft Gripper* [2], was introduced in 1978. This latter device was a gripper made of two tentacle-like fingers with ten phalanges each that could envelop virtually any shape without any control or sensors. The single input force driving the finger was distributed to the numerous phalanges by a tendon routed around several pulleys cleverly placed along the phalanges. Many other well-known examples of underactuated grasping devices driven by tendons can now be found in the literature, e.g., [3]–[5]. Another common type of transmission in underactuated fingers is based on a linkage instead of a tendon but the underlying principles stay the same. A typical grasp sequence of an underactuated finger with three phalanges is illustrated in the upper part of Fig. 1. In this example, a single actuation torque is distributed by a mechanism (not shown in this figure) to the three phalanges. Passive elements such as springs typically constrain the finger to a specific shape before a contact with an object happens (this is referred to as the preshaping phase). The intrinsic ability of self-adaptive fingers to adapt themselves to objects makes their closing motion and final configuration dictated mostly by the shape of these objects, not by the motion of the actuator, which is instead typically force controlled. Thus, since one has only one actuator but several contact forces, these forces are not fully controllable (they are not independent) and moreover, their locations are usually not exactly known at least not without additional sensors.

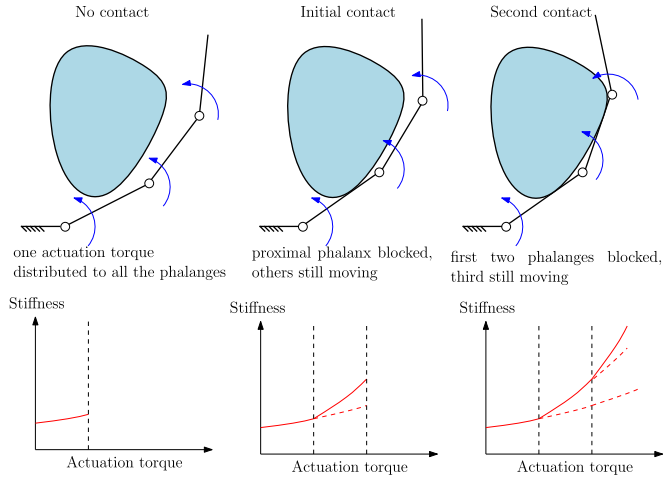

Fig. 1. Typical closing sequence of an underactuated finger.

Several types of sensors can be used to provide tactile feedback and, depending on the application, they can have a critical role in the control architectures of the robotic fingers to which they are attached. In addition to the conventional sensors typically found connected to the actuators, such as joint encoders and electrical measurement devices (current/voltage),

Manuscript received May 19, 2015; revised November 10, 2015, March 3, 2015, and May 26, 2015; accepted June 3, 2016. Date of publication July 9, 2016; date of current version December 13, 2016. Recommended by Technical Editor H. Moon. This work was supported by the National Science and Engineering Research Council and by the Fonds de recherche du Québec—Nature et Technologies and the Canadian Foundation for Innovation.

The authors are with the Department of Mechanical Engineering, Polytechnique Montreal, Montreal, QC H3C 3A7, Canada (e-mail: bruno.belzile@polymtl.ca; lionel.birglen@polymtl.ca).

Color versions of one or more of the figures in this paper are available online at http://ieeexplore.ieee.org.

Digital Object Identifier 10.1109/TMECH.2016.2589546

tactile sensors are often desirable. In particular, they can be used to control the magnitudes of the contact forces as well as precisely measure their locations [1], [6]. Mechatronic hand prostheses and teleoperated devices are examples of commonly found applications where they are almost deemed mandatory [7], [8]. The data they provide to the control system can be the basis of a whole upper level of cognitive control, aiming at, for instance, assessing grasp stability, performing object recognition, detecting slippage, or collision, etc. [9]–[11]. A recently growing trend, very close to classical tactile sensing, is the design and prototyping of "robot skins" and sensor arrays [12]. These skins typically cover large areas of a robot (which might include the fingers) to provide spatial localization of contact forces, with the objective of adding compliance and safety in human–robot collaboration tasks. If the usefulness of tactile information is rarely doubted, it can be noted that there exists a plethora of tactile sensing technologies. Indeed, these sensors are typically classified in broad categories based on the physical phenomenon on which they rely to detect the applied pressure. For instance, capacitive, piezoresistive, piezoelectric, inductive, and optoelectric tactile sensors exist [13]. However, whatever the technology used and despite their usefulness, tactile sensing suffers from a few enduring weaknesses, namely invasive and intricate designs, prohibitive costs, and fragility.

To circumvent these issues, another sensing technique is presented in this paper which takes advantage of the peculiar mechanical properties of underactuated fingers. As figuratively illustrated in the lower half of Fig. 1, it was experimentally noticed by Belzile and Birglen [14] that the stiffness of an underactuated finger as seen from its sole actuator is generally nonlinear and a function of the contact locations on the finger. Indeed, once a first contact with an object is established, to continue the closing motion of the finger, the actuator has to increase the torque it provides. This variation can often be significant and it was noticed that the magnitude of this stiffness increase was related to the location of this first contact. Thus emerges the possibility of tactile sensing based on this phenomenon. As will be shown in the first part of this paper, the authors were successfully able to establish an analytical correspondence between the stiffness of an underactuated finger and the location of a single point of contact with the finger. While subsequent contacts also cause stiffness variations that can be measured at the actuator, it is not the focus of this paper. However, the method presented here could be adapted as briefly explained in the conclusion. It should be mentioned that the stiffness analysis of a robotic finger in general [15] or even an underactuated one [16]–[18] is nothing new and several examples can be found in the literature. However, in the case discussed in this paper, the stiffness of the underactuated finger is considered as seen from its actuator point of view and, to the best of the authors' knowledge, this is the first time such model is used to obtain tactile data. The algorithm presented here follows prior work [19] on double-tendon underactuated fingers where a return cable was used instead of compliant elements, conversely to this paper. With this particular architecture, negative torque compensation at the interphalanx joints was used to estimate the contact location instead of measuring the instantaneous stiffness. Indeed,

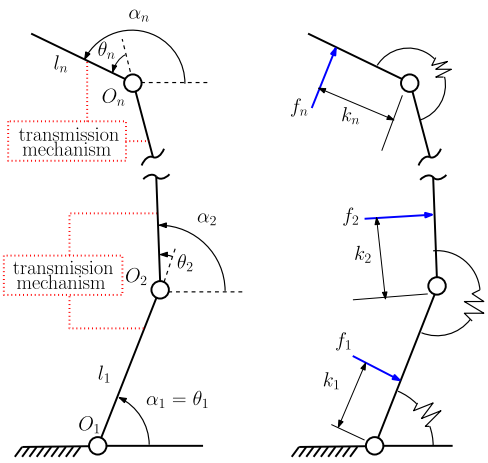

Fig. 2. Underactuated finger with n phalanges.

a preconstrained return tendon distributed a negative torque at the interphalanx joints, extending the finger and stopping the phalanges at their mechanical limit. The actuation torque was then use to overcome these negative torques and induce motion. After a contact was made, a certain increase of the actuation torque was needed to resume motion. Its value being a function of the contact location, it was thus possible to estimate the latter by measuring the torque variation at the actuator. While the measured phenomenon is different here, the basic idea, which is performing tactile sensing with proprioceptive measurements, remains the same.

Ultimately, the objective here is to propose a method to use proprioceptive (internal) sensors such as these attached to the actuator of the finger instead of exteroceptive sensors to obtain as much contact information as possible. This would allow for a low cost, yet reasonably efficient alternative to tactile sensors [8]. One should note that proprioceptive sensors have already been used to determine the location of contact points between a robotic finger and an unknown object but with fully actuated fingers, e.g., [20]–[24]. This paper aims at filling that gap and presenting algorithms usable with most architectures of underactuated fingers with compliant elements located at the interphalanx joints, with the objective of precisely locating a single contact on any phalanx after the proximal one. It should be noted that examples using accelerometers [25] and electromagnetic trackers [26] can also be found in the literature, but these sensors are uncommonly found inside the fingers and do not use data from the actuator. This technique had yet to be adapted to underactuated designs.

II. Modeling of Underactuated Robotic Fingers

A. Notations and Hypotheses

To simplify the modeling of underactuated fingers presented in this paper, two sets of angles are used, namely α_i and θ_i, which are, respectively, the absolute and relative joint angles of the phalanges, as illustrated in Fig. 2. One useful velocity vector must also be defined, namely $\dot{\boldsymbol{\theta}} = [\dot{\theta}_1 \quad \dot{\theta}_2 \quad \dots \quad \dot{\theta}_n]^T$. This velocity vector contains the interphalanx joint velocities, and

its antiderivative is $\boldsymbol{\theta}$. The object to be grasped is considered to be significantly stiffer than the finger and immovable with respect to the finger base so the latter will envelop it rather than pushing it away. Furthermore, the contact force on each phalanx is assumed to be unique and normal to the surface of this phalanx. Finally, dynamic phenomena are neglected in favor of a simpler kinetostatic analysis since the kinetic energy of the system is typically low during a grasp. The analysis performed in the subsequent sections of this paper is valid for underactuated fingers that can be modeled by a transmission matrix, as shown in [1], which cover most if not all current tendon- or linkage-driven designs. Finally, torque and position measurements at the actuator are assumed to be available as both are used by the proposed algorithm.

B. Contact Forces

The contact forces between a self-adaptive finger with n phalanges and an arbitrary object can be related to the Jacobian and transmission matrices of this finger [1]

$$\mathbf{f} = \mathbf{J}^{-T}\boldsymbol{\tau} = \mathbf{J}^{-T}\mathbf{T}^{*T}\mathbf{t} \tag{1}$$

with $\mathbf{t} = \begin{bmatrix} T_a & T_1 & T_2 & \dots & T_n \end{bmatrix}^T$, and where $\mathbf{J}$ is the aforementioned Jacobian matrix, $\mathbf{T}^*$ the transmission matrix, T_a the single actuator torque, T_i the torque generated by the spring at the ith joint of the finger (see point O_i in Fig. 2) and $\mathbf{f}$ the contact force vector. The Jacobian matrix can be shown to depend solely on the number of phalanges, their lengths l_i, and the locations of the contact forces k_i. It is defined for a three-phalanx finger by

$$\mathbf{J}^{-T} = \begin{bmatrix} \frac{1}{k_1} & \frac{-\beta_2}{k_1} & \frac{(\beta_2-1)-\psi_3+(\beta_2-1)(\beta_3-1)}{k_1} \\ 0 & \frac{1}{k_2} & \frac{-\beta_3}{k_2} \\ 0 & 0 & \frac{1}{k_3} \end{bmatrix} \tag{2}$$

where

$$\beta_i = 1 + (l_{i-1}\cos\theta_i)/k_i \text{ and } \psi_3 = (l_1\cos(\theta_2+\theta_3))/k_3. \tag{3}$$

It is important to emphasize that k_i, illustrated in Fig. 2, is the distance from point O_i to the contact location on this phalanx and should not be confused with the stiffness K_i used later in this paper. In the case of a two-phalanx finger, the Jacobian matrix is simply the upper left 2×2 submatrix of (2). The other characteristic matrix of an underactuated finger, namely the transmission matrix, depends on the geometry of the transmission mechanism used to distribute the actuation torque. There are many possible solutions for this but, as previously mentioned, the two most commonly found are tendon-driven [see Fig. 3(a)] and linkage-driven [see Fig. 3(b)] designs [1]. For both of the latter, if torsion springs are located between the phalanges, as illustrated in Fig. 2, the transmission matrix $\mathbf{T}^*$ can be defined as

$$\mathbf{T}^* = \begin{bmatrix} \boldsymbol{x} & \mathbf{I} \end{bmatrix}^T \tag{4}$$

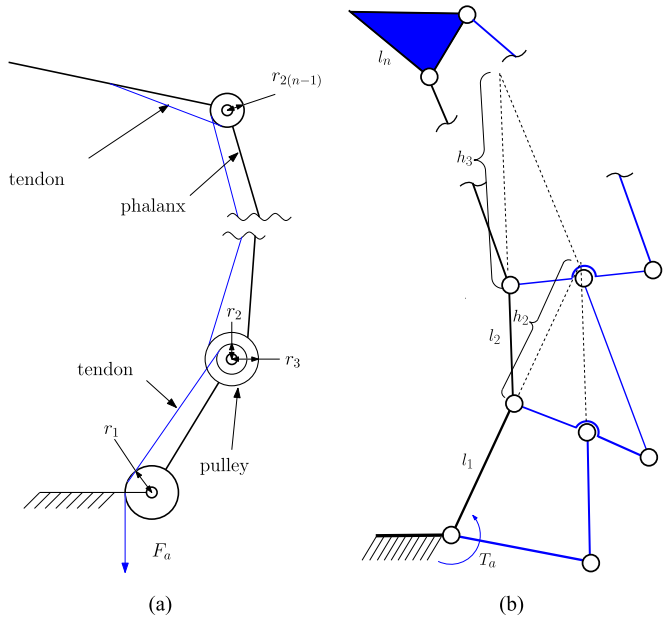

Fig. 3. Geometries and transmissions of typical underactuated fingers. (a) Tendon-driven $T_a = r_1 F_a$. (b) Linkage-driven.

where the matrix $\mathbf{I}$ is the $n \times n$ identity matrix and the vector $\boldsymbol{x}$ is defined as $\begin{bmatrix} 1/X_1 & -X_2/X_1 & \dots & -X_n/X_1 \end{bmatrix}^T$. The scalars X_i are the transmission factors that depend on the transmission mechanism, see [1] for numerous examples. For several standard driving mechanisms, such the ones shown in Fig. 3(a) and (b), X_1 is equal to 1. From this standard transmission matrix, the vector $\boldsymbol{\tau}$ in (1) can be computed as

$$\boldsymbol{\tau} = -\mathbf{K}(\boldsymbol{\theta} - \boldsymbol{\theta}_0) + \boldsymbol{x}T_a. \tag{5}$$

Indeed, the components of the vector $\boldsymbol{\tau} = [\tau_1, \dots, \tau_n]^T$ are the equivalent torques at the interphalanx joints, i.e., the sum of torques due to the springs and the distributed actuation torque, as opposed to the components of $\boldsymbol{t}$ that are the previous terms but listed separately. In (5), $\mathbf{K}$ is a diagonal stiffness matrix with K_j being the jth element on the diagonal modeling the stiffness of the spring located at O_j. The subscript 0 in (5) denotes the state at rest, i.e., without any input force.

C. Preshaping

The preshaping of a self-adaptive finger is defined by its motion before any contact is made with an object [27] and [28]. While there is no contact force during this stage of the grasping sequence, it is still possible to extract useful information from (1). Knowing that $\mathbf{f}$ is a null vector when there is no external force, it becomes clear that $\boldsymbol{\tau}$ must lie in the null space of $\mathbf{J}^{-T}$. The matrix $\mathbf{J}^{-T}$ been always upper triangular, the only solution always valid even if $\mathbf{J}^{-T}$ is not constant (which is the case during preshaping) is $\mathbf{0}$. Thus, for a general n-phalanx finger, it can be concluded that every equivalent torque at the phalanx joints are null, i.e.,

$$\tau_i = 0 \text{ for } i = 1, \dots, n. \tag{6}$$

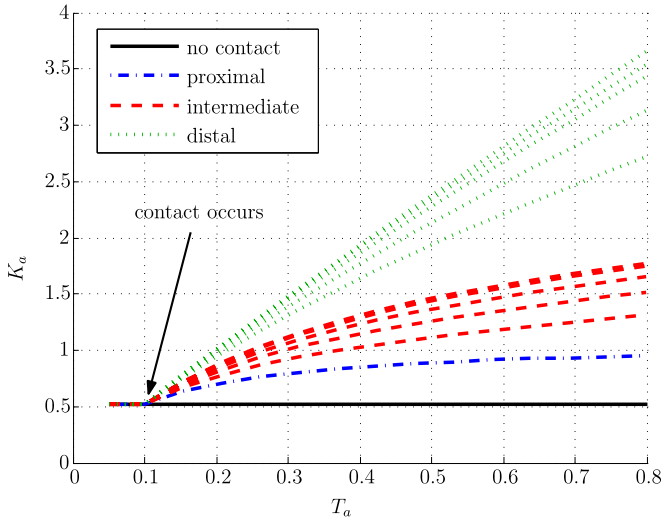

Fig. 4. Stiffness with or without contact on a 3 DOF finger.

TABLE I
GEOMETRIC PARAMETERS OF THE THREE-PHALANX FINGER EXAMPLE

l_1	1.00	r_1	0.10	r_4	0.04
l_2	0.75	r_2	0.08	$\theta_{i,0}$	$\pi/6$
l_3	0.50	r_3	0.06	K_i	1.0

This also holds at the initial instant of the first contact. To compute the preshaping motion of the finger, the system of n equations defined by (6) must be solved. By comparing the expected stiffness (without contact) to the measured current stiffness, it is possible to establish if contact is made or not, as the stiffness K_a after contact is typically significantly larger than its no-contact counterpart. This stiffness K_a is defined as the global stiffness of the mechanism as seen from the single actuator, namely

$$K_a = (T_a - T_{a,0})/(\theta_a - \theta_{a,0}) \tag{7}$$

where T_a, θ_a, $T_{a,0}$, and $\theta_{a,0}$ are, respectively, the current actuation torque, position, and their original values at rest. For a tendon-driven finger, θ_a is usually the angle of the base pulley. The ratio between the base pulley and the actuator angles is assumed to be 1. A numerical example is given in Fig. 4, where the solid black curve at the bottom is the stiffness K_a as a function of the input torque during a closing motion without any contact. The geometric parameters of the finger used in this example are listed in Table I. It should be noted that K_a is not always constant for this type of motion as in this example, it depends on the transmission mechanism used. If the transmission factors X_i are constant, then K_a will also be constant. For the other curves in Fig. 4, a contact is made after a certain amount of preshaping as computed using (6). Each curve corresponds to a different initial contact location on the finger. The lines with the same dashed style represent contact locations evenly distributed along the same phalanx. The first curve above the solid one is for a contact on the first phalanx. The ones near the top of the figure represent a contact on the distal phalanx. As this example indicates, the change of the stiffness K_a strongly depends on the contact location. Solving the inverse problem, i.e., finding this location based on the observed stiffness is the objective of this paper and is realized through a thorough analysis of the stiffness that follows. Several examples for fingers with two and three phalanges will then be presented.

III. PRELIMINARY ANALYSIS

In order to establish where the original contact happens on an underactuated finger, one does not only need K_a but also the instantaneous stiffness after contact K_c defined as

$$K_c = dT_a/d\theta_a. \tag{8}$$

In the case of K_c, if no motion is possible after contact, its magnitude goes to infinity, conversely to K_a, which will always have a finite numerical value if there was a motion of the finger before contact. To compute K_c, one has to differentiate (1) with respect to T_a. However, before doing so, one can simplify (1) by reducing $\mathbf{J}^{-T}$ to the $(n-1)$ rows, where the f_i is equal to zero as also shown in [19]. Indeed, when there is only one contact with an object, only one element of $\mathbf{f}$ is non-zero. Thus, if $\mathbf{J}^{-T}$ is defined as

$$\mathbf{J}^{-T} = \begin{bmatrix} \mathbf{j}_1 & \mathbf{j}_2 & \cdots & \mathbf{j}_k & \cdots & \mathbf{j}_n \end{bmatrix}^T \tag{9}$$

and one can define $\mathbf{J}_i^*$ (a submatrix of $\mathbf{J}^{-T}$ with only $n-1$ lines) for a contact on the kth phalanx as

$$\mathbf{J}_i^* = \begin{bmatrix} \mathbf{j}_1 & \mathbf{j}_2 & \cdots & \mathbf{j}_{k-1} & \mathbf{j}_{k+1} & \cdots & \mathbf{j}_n \end{bmatrix}^T. \tag{10}$$

Also, when an undefined k_i appears in this matrix (it is deemed undefined because there is no contact on the associated phalanx), a Gaussian elimination must be used to get rid of this k_i. In the case of a three-phalanx finger, one can then compute the three $\mathbf{J}_i^*$ corresponding to a contact on, respectively, the proximal, intermediate, and distal phalanges. The three different $\mathbf{J}_i^*$ obtained are

$$\mathbf{J}_1^* = \begin{bmatrix} 0 & 1 & 0 \\ 0 & 0 & 1 \end{bmatrix}, \mathbf{J}_2^* = \begin{bmatrix} 1 & -\beta_2 & 0 \\ 0 & 0 & 1 \end{bmatrix}, \tag{11}$$

$$\text{and } \mathbf{J}_3^* = \begin{bmatrix} 1 & 0 & -\beta_3 - \psi_3 \\ 0 & 1 & -\beta_3 \end{bmatrix}. \tag{12}$$

For a two-phalanx finger, only the first two elements of the first row of the first two $\mathbf{J}_i^*$ defined above are used. In both cases, a simplified form of (1) is obtained, i.e.,

$$\mathbf{J}_i^* \boldsymbol{\tau} = \mathbf{0}. \tag{13}$$

After differentiating with respect to T_a, this becomes

$$(d\mathbf{J}_i^*/dT_a)\boldsymbol{\tau} + \mathbf{J}_i^*(d\boldsymbol{\tau}/dT_a) = \mathbf{0}. \tag{14}$$

The equivalent torque vector $\boldsymbol{\tau}$ been null during preshaping, only the second element of this equation remains at the instant of contact. By expanding the derivative, one obtains

$$\mathbf{J}_i^* \left((\mathbf{G} - \mathbf{K})d\boldsymbol{\theta}/dT_a + \boldsymbol{x}\right) = \mathbf{0} \tag{15}$$

where $\mathbf{G}$ is the product of T_a and the mathematical Jacobian of $\boldsymbol{x}$ with respect to $\boldsymbol{\theta}$, i.e., $\mathbf{G} = \frac{\partial \boldsymbol{x}}{\partial \boldsymbol{\theta}} T_a$. Furthermore, one also has

$$d\theta_a/dT_a = \boldsymbol{x}^T d\boldsymbol{\theta}/dT_a = 1/K_c. \tag{16}$$

Equation (15) provides only $n-1$ equations. To have a fully determined system, one has to add the contact closure equation, which depends on the phalanx where the contact happens. This equation is obtained by differentiating the geometric closure equation from the base of the finger to the point of contact on the kth phalanx. Its general form is the following:

$$\mathbf{\Gamma}_i^T \, d\boldsymbol{\theta}/dT_a = 0 \tag{17}$$

where $\mathbf{\Gamma}_i$ contains coefficients that are functions of the phalanx in contact and location of the latter. The possible values of $\mathbf{\Gamma}_i$ are detailed below. It should be noted that there is a different $\mathbf{\Gamma}_i$ for each phalanx. For example, if the contact occurs on the second phalanx, $\mathbf{\Gamma}_2$ should be used. Finally, combining (15), (16), and (17), one can compute the instantaneous stiffness after contact, namely

$$K_c^{-1} = \frac{d\theta_a}{dT_a} = \boldsymbol{x}^T \begin{bmatrix} \mathbf{J}_i^*(\mathbf{K}-\mathbf{G}) \\ \mathbf{\Gamma}_i^T \end{bmatrix}^{-1} \begin{bmatrix} \mathbf{J}_i^* \\ \mathbf{0}^T \end{bmatrix} \boldsymbol{x}. \tag{18}$$

The vector $\mathbf{\Gamma}_i$, which defines the contact configuration, can be computed from simple geometric equations. First, assuming that the contact location is fixed relatively to the base of the finger, the geometric closure equations at the instant of contact and after contact (on the ith phalanx) are

$$k_i \sin\alpha_i + \sum_{j=1}^{i-1} l_j \sin\alpha_j = k_{i,c} \sin\alpha_{i,c} + \sum_{j=1}^{i-1} l_j \sin\alpha_{j,c} \tag{19}$$

$$k_i \cos\alpha_i + \sum_{j=1}^{i-1} l_j \cos\alpha_j = k_{i,c} \cos\alpha_{i,c} + \sum_{j=1}^{i-1} l_j \cos\alpha_{j,c} \tag{20}$$

where $\alpha_i = \sum_{j=1}^{i} \theta_j$. The subscript c stands for the instant of contact. By combining these two equations, one obtains

$$k_i = \frac{\sum_{j=1}^{i-1} l_j(\sin(\alpha_j - \alpha_{i,c}) + \sin(\alpha_{i,c} - \alpha_{j,c}))}{\sin(\alpha_{i,c} - \alpha_i)}. \tag{21}$$

Differentiating the latter expression and evaluating its value at the instant of contact yields

$$-\frac{d\alpha_i}{dT_a} = \sum_{j=1}^{i-1} \lambda_j^i \frac{d\alpha_j}{dT_a} = \sum_{j=1}^{i-1} \frac{l_j \cos(\alpha_j - \alpha_{i,c})}{k_i} \frac{d\alpha_j}{dT_a}. \tag{22}$$

With $\lambda_i^i = 1$, (22) becomes

$$\sum_{j=1}^{i} \lambda_j^i \frac{d\alpha_j}{dT_a} = 0. \tag{23}$$

Then, by using the definition of α_j, one can obtain the general vector $\mathbf{\Gamma}_i$ for a contact on the ith phalanx, i.e.,

$$\mathbf{\Gamma}_i = \left[\sum_{j=1}^{i} \lambda_j^i \;\; \sum_{j=2}^{i} \lambda_j^i \;\; \dots \;\; \sum_{j=i-1}^{i} \lambda_j^i \;\; \lambda_i^i \right]^T. \tag{24}$$

The vector $\mathbf{\Gamma}_i$ is completed by zeros if $i < n$. For contacts on the first, second, and third phalanges, the resulting expressions of $\mathbf{\Gamma}_i$ are

$$\mathbf{\Gamma}_1 = 1, \mathbf{\Gamma}_2 = \begin{bmatrix} \beta_2 & 1 \end{bmatrix}^T, \mathbf{\Gamma}_3 = \begin{bmatrix} \beta_3 + \psi_3 & \beta_3 \; 1 \end{bmatrix}^T. \tag{25}$$

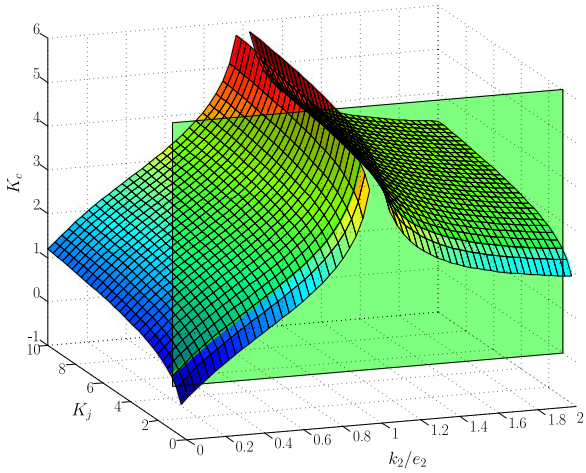

Fig. 5. K_c as a function of the initial contact location k_2 and the stiffnesses of the springs, assumed identical ($K_j = K_1 = K_2$).

It should be noted that the variable k_1 does not appear in $\mathbf{\Gamma}_1$, meaning that the exact contact location along the proximal phalanx has no effect on the overall stiffness, as seen from the actuator. Indeed, the closing motion remains the same afterward. Examples of the values of the stiffness K_c of fingers with two and three phalanges will be presented in the following sections, as computed from (18), to illustrate how it changes as a function of the contact location and other parameters.

IV. Two-Phalanx Fingers

The first category of underactuated fingers considered here are two-phalanx designs. The vector $\boldsymbol{x}$ is defined by $\boldsymbol{x} = [1/X_1 \;\; -X_2/X_1]^T$. For a tendon-driven transmission [see Fig. 3(a)], $X_1 = 1$ and $X_2 = -r_2/r_1$. In the case of a linkage-driven finger [see Fig. 3(b)], $X_1 = 1$ and $X_2 = -h_2/(h_2 + l_1)$. One important property of two-phalanx fingers is that there exists a contact location on the distal phalanx where there is a static equilibrium of the 2 degrees of freedom (DOF) mechanism constrained by a single contact. Thus, even if the input torque increases, there will not be any motion, only a contact force increase. This location e_2 depends on the configuration of the finger. By having a closer look to (18), the stiffness is infinite if

$$\begin{bmatrix} \mathbf{J}_i^{*T} & \mathbf{0} \end{bmatrix}^T \boldsymbol{x} = \mathbf{0}. \tag{26}$$

Thus, e_2 can be computed, which yields

$$e_2 = (-l_1 \cos\theta_2 X_2)/(1 + X_2). \tag{27}$$

Examples of K_c as a function of the contact location for a tendon-driven 2 DOF finger are shown in Fig. 5. In this figure, the parameters are the same as in Table I for the intersection with the green plane. For the rest of the surface, the stiffnesses of the torsion springs (K_1 and K_2, both equal) change.

V. Three-Phalanx Fingers

In the case of three-phalanx fingers, the kinetostatic analysis of the finger after contact is more complex, but the method stays

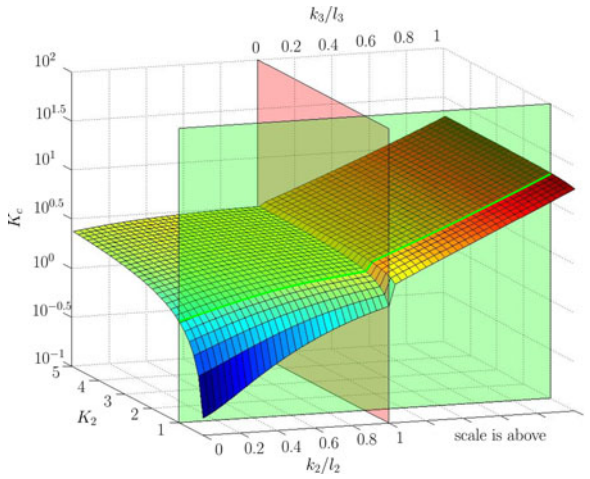

Fig. 6. K_c for a 3 DOF finger as a function of K_2 and contact locations.

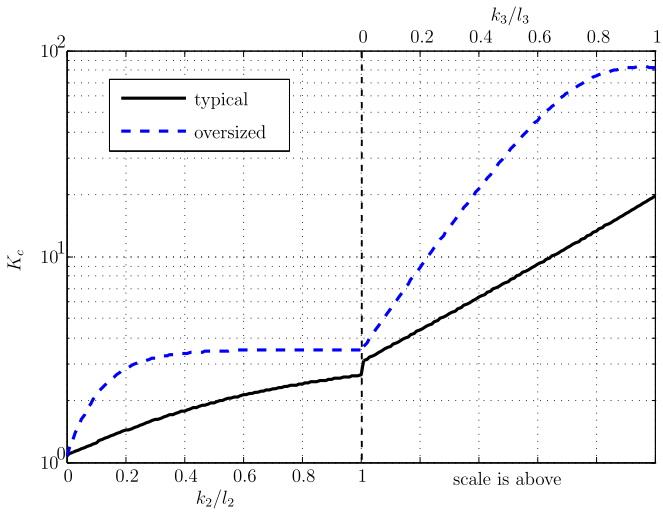

Fig. 7. K_c as a function of the initial contact location for two designs.

the same. The vector $\boldsymbol{x}$ is in this case defined by

$$\boldsymbol{x} = [1/X_1 \ -X_2/X_1 \ -X_3/X_1]^T. \tag{28}$$

The transmission factor X_3 is $-(r_2 r_4)/(r_1 r_3)$ for the tendon-driven finger [see Fig. 3(a)] and $-(h_3 h_2)/((h_2 + l_1)(h_3 + l_2))$ for the linkage-driven finger [see Fig. 3(b)]. All coefficients in the expression of K_c in (18) obviously have an effect on the instantaneous stiffness curve. However, for typical designs some of them do not seem to significantly impact the shape of the curve, only the final value of K_c, as illustrated in Fig. 6 with the parameters of Table I and different values of K_2. It should be noted that the contact location axis of this figure is normalized with respect to the phalanx length and not the equilibrium position. In this figure, K_2 ranges from five times smaller to five times greater than its initial value. Some special contact configurations can also be considered, such as multiple contact locations yielding the exactly same after-contact stiffness. For instance, let us consider the two possible scenarios shown in Fig. 7. First, for the typical finger used in this paper, the instantaneous stiffness corresponds to the solid curve. In the second case corresponding to an oversized design where l_1 is half its original size, l_2 is three times longer, and l_3 is six times longer. Then, K_c actually decreases after a peak value on both phalanges. This situation makes it impossible to distinguish contacts on several locations on this finger. Again, this should be avoided by carefully designing the finger. Conversely to the 2 DOF fingers, it is possible to see from simulations that the contact location leading to the maximal stiffness on the second phalanx, e_2, does not yield an infinite stiffness because only the first and second phalanges are stopped. The distal phalanx itself continues its closing motion when the input torque increases.

VI. Tactile Sensing Algorithm

From the analysis presented in the previous section, it can be concluded that it is possible to extract contact location from measuring the stiffness as seen by the actuator of the finger. The first and simplest information being obviously whether a contact with an object happened or not. One can also create

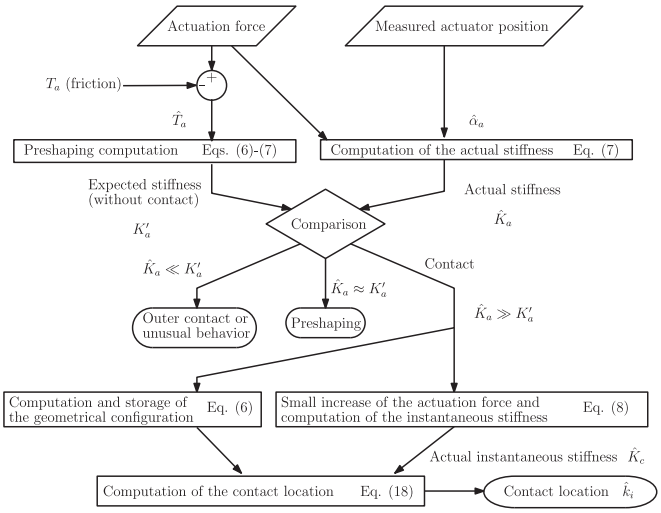

Fig. 8. Algorithm for contact location estimation.

virtual tactile sensors by combining computation algorithms to the data coming from the internal torque and position sensors of the actuator. From these virtual sensors, the contact locations and the applied forces can be estimated. However, one limitation is that without any actual tactile sensor located on the proximal phalanx, if a contact there can be detected by the change of stiffness, it is impossible to know exactly where it is made on this phalanx. With the subsequent phalanges, a significant variation of stiffness K_c makes it possible to estimate the contact location. The algorithm schematically presented in Fig. 8 shows how the contact location can be computed. With the contact location known, it is then possible to estimate the magnitudes of the associated forces using (1).

In the algorithm presented in Fig. 8, the only sensors necessary are at the actuator: a torque sensor (or equivalently, a current sensor) and a position sensor. With the actuation torque, the expected stiffness K'_a of the finger without contact can be

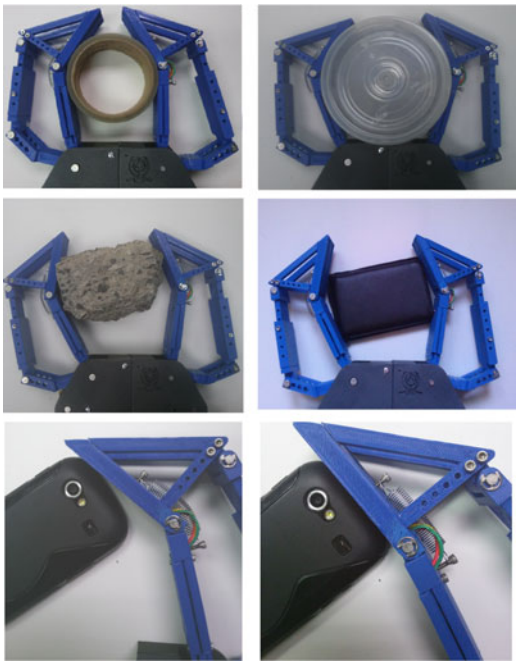

Fig. 9. Examples of grasps with a 2 DOF linkage-driven finger.

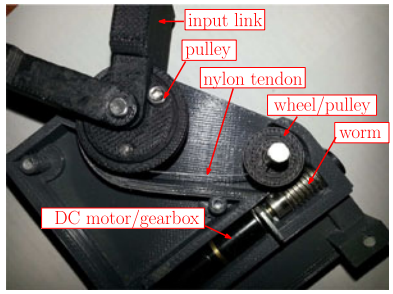

Fig. 10. Driving mechanism.

TABLE II
GEOMETRIC PARAMETERS OF THE PROTOTYPE

l_1	1.00	b	0.10	$\theta_{1,0}$	$\pi/4$
l_2	0.75	c	0.08	$\theta_{2,0}$	0
a	0.50	ϕ	0.06		

computed. By also measuring the actuator position, the actual stiffness $\hat{K}_a$ can be computed too. The next step is to compare these two values. If they are identical, or at least reasonably close, then there is no contact between the finger and any object. If the measured stiffness is smaller, then an unusual situation is occurring, for example, a failure of the mechanism or a contact on the finger's back. On the other hand, a more meaningful situation is when the measured stiffness is greater than expected, meaning that a contact has occurred. By computing the geometric configuration the instant before contact and performing a small increase of the input force to compute the instantaneous stiffness $\hat{K}_c$, it is possible to estimate the contact location with (18). The contact locations k_i must be computed for every phalanx with only one giving a possible solution (i.e., $0 < k_i < l_i$). When each matrix is replaced by the one corresponding to the tested phalanx, k_i becomes the sole unknown.

It should be noted that the proprioceptive tactile sensing algorithm presented in this paper can be adapted to fully actuated fingers. Indeed, while proprioceptive data from only one actuator are needed, additional actuators with torque and position sensors can be incorporated into the algorithm. In that case, the transmission matrix defined in (4) becomes the identity matrix and the term $\boldsymbol{x}T_a$ in (5) becomes the actuated joint vector. Then, the global and instantaneous stiffnesses K_a and K_c must be computed for each actuator.

VII. EXPERIMENTAL VALIDATION

To validate the proposed tactile sensing algorithm, several experiments were performed with a 2 DOF linkage-driven finger prototype. This prototype is shown in Fig. 9. A Maxon RE10 brushed 1.5 W dc motor is used to drive the linkage. It is coupled to a 64:1 gearbox and a 256 cpt optical encoder. Between the actuator gearbox and the input link of the finger are a 20:1 wheel and worm gear as well as two pulleys coupled by a nylon cable, as shown in Fig. 10. The dimensions of the finger are presented in Table II. Additionally, a Maxon LSC 30/2 motor controller is also used. A Hall effect sensor is located in the joint between the proximal and distal phalanges for improved position feedback, but it is not necessary to use the algorithm presented in this paper. A nylon tendon is used between the actuator and the pulley at the base of the finger to transmit the torque. The stiffness of this tendon is taken into account in the algorithm, as described in [14]. Experimental data were collected with this prototype to quantify the precision of the tactile sensing algorithm. First, the linkage was tested without the actuator, the wheel, and the worm gear. The input force was directly applied to the base pulley attached to the input link a. The variation angle $\Delta\theta_a$ was then measured to compute the instantaneous stiffness. The results for different points of contact along the distal phalanx are shown in Fig. 11. As predicted, a significant increase of the instantaneous stiffness can clearly be observed as the distance k_2 is increased. Moreover, the asymptotic nature of the curve makes it possible to still have a fairly precise estimation even with a significant deviation of the instantaneous stiffness compared to the one predicted by the model.

In a second experimental phase, the dc actuator and the reduction stages were added. In each test, a small actuation torque T_a was used to make contact with the object at which time the actuated link angle θ_a was recorded. Since, in the absence of a spring at the base joint, K_1 is equal to zero, the driving torque was therefore, only opposed by friction. The latter was subtracted from the measurements after a first full closing of the finger without an object during which it was recorded, as illustrated in Fig. 12. Then, still in contact with the object, the actuation torque was increased to produce an observable variation of the angle θ_a, allowing to compute $\hat{K}_c$ and use its value to estimate k_i. The lower dashed and dotted lines in Fig. 12

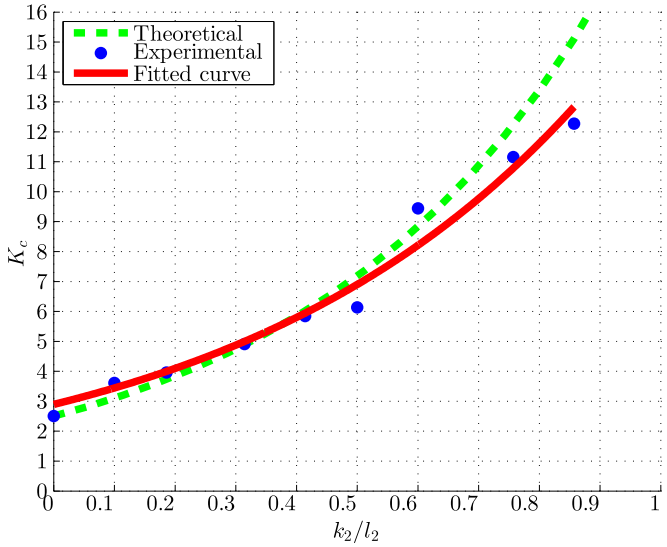

Fig. 11. Experimental instantaneous stiffness curve.

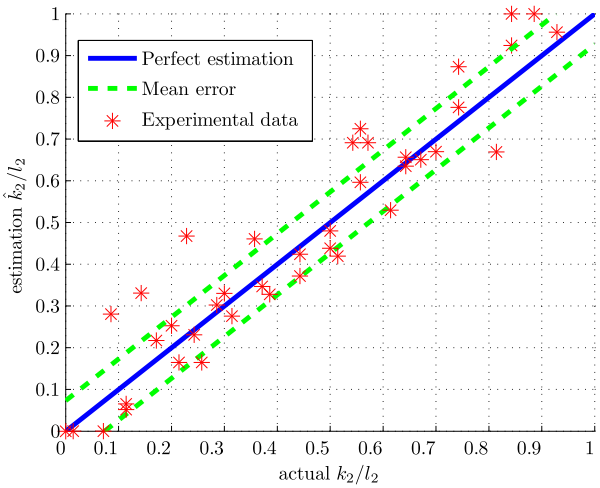

Fig. 13. Actual contact locations versus estimated values.

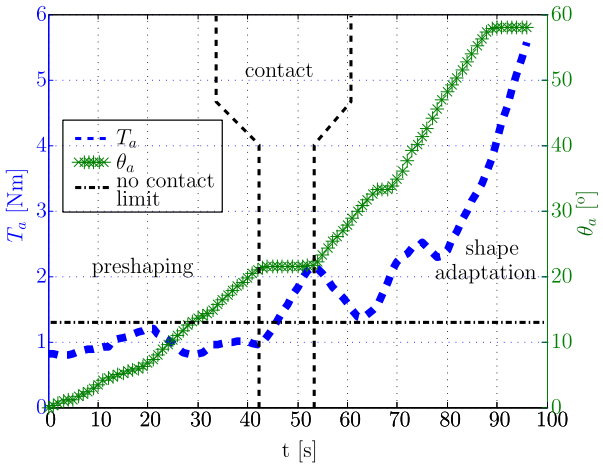

Fig. 12. Actuator torque and angle during a closing sequence.

represent the actuation torque threshold under which no contact is recorded. This specific torque stems from the friction within the mechanism. Its value is the one subtracted from the measured torque and used by the algorithm. As also visible in Fig. 12, an increase of the actuation torque is needed after the initial contact to resume motion. The actual initial contact location was measured visually with a picture taken above the setup and also with a calliper. During the experiments, it was clearly observed that the measured actuator angle depends on the contact location and the driving torque.

Different grasping scenarios were tried out. Among them, power grasps where the proximal phalanx comes first in contact with the object (illustrated in the upper left of Fig. 9). However, one limitation is that without any actual tactile sensor located on the first phalanx, while a contact can be detected by the change of stiffness, it is impossible to determine where exactly it is made. As shown in Section III, the reason is that the associated variable k_1 does not appear in the equation of the stiffness as seen by the actuator. While being unable to locate this type of contact, the algorithm was still able to determine that a contact occurred with this phalanx nearly every time due to the large increase of stiffnesses. Twenty-five trials were performed for the proximal phalanx, with a success rate of 84%. For the second phalanx, the algorithm was able to compute a fairly precise approximation of the contact location with a mean error of 7.3% (5.1 mm) and a standard deviation of 6.0% (4.2 mm) measured during 40 experiments with 10 different objects and a punctual point of contact generated with a cylinder with a small diameter. Fig. 13 illustrates results from these experiments performed with different contact locations along the distal phalanx. Dots within the dashed lines in this figure show an error smaller than the mean error. A perfect linear contact along the second phalanx, as illustrated in the lower right picture of Fig. 9, is also a possible scenario. If the limits of the linear contact are located below the equilibrium point e_2, only the upper vertex is detected as the finger only stays in contact with this point if the driving torque is increased. If the limits are located after e_2, the lowest one is detected, as the angle θ_2 decreases. Otherwise, if e_2 is within the limits of the linear contact, the finger will remain completely rigid and the estimated contact point will be e_2.

The discrepancies shown in Fig. 13 can be attributed to practical limitations. First, as with most if not all mechanical systems, a perfect friction compensation is impossible. Thus, with the simple model used here to reduce its impact, a deviation from the theoretical model must be anticipated. Second, the stiffness coefficients of the springs can create significant errors if they are not carefully measured since the instantaneous stiffness is proportional to them. Additionally, the fact that the linear springs used in the finger are not perfect torsion springs also has an impact. Finally, to complete the experimental validation, the influence of the preshaping was studied by changing the location of the initial contact on the distal phalanx for different angles θ_1 (five different k_2, five different θ_1). Estimation errors were computed for each one of these 25 configurations, cf., Fig. 14.

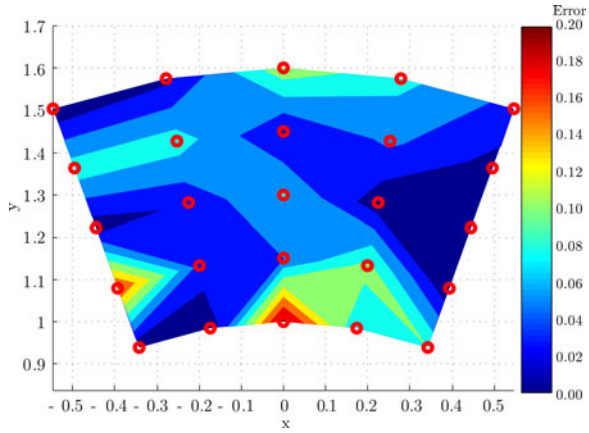

Fig. 14. Estimation error as a function of the initial contact position.

As it can be seen, the estimation error is on average 4.6% and is generally not impacted by the preshaping.

VIII. Conclusion

From the simulations and the experimental data presented in this paper, the authors conclude that it is possible to extract a significant amount of tactile data solely from proprioceptive sensors attached to the actuator of an underactuated finger. Indeed, variations in the perceived stiffness at the actuator can be linked to the actual contact location on an underactuated finger with compliant elements at its joints. A careful stiffness model is the basis for the estimation algorithm connecting these variables. While some cases might still require sensors, such as an initial contact on the proximal phalanx, an interesting amount of tactile information can be computed and established with a virtual sensor based on typically already available data. Future work will focus on how to improve the precision of the algorithm and the detection of a subsequent contact, which is predicted to be possible using a similar model as the one proposed here but including the parameters of the first contact detected. Indeed, for a 3 DOF finger, the matrix $\mathbf{J}^*$ becomes a line vector when there are two simultaneous contacts and the vector $\mathbf{\Gamma_i}$ a matrix. Therefore, the system of equations stays fully determined. The greater stiffness generated by a second contact may render it more difficult to locate this additional contact, but an optimization of the instantaneous stiffness curve would probably solve this problem.

References

[1] L. Birglen, T. Laliberté, and C. Gosselin, *Underactuated Robotic Hands (Springer Tracts in Advanced Robotics)*, B. Siciliano, O. Khatib, and F. Groen, Eds. Berlin, Heidelberg: Springer-Verlag, 2008.

[2] S. Hirose and Y. Umetani, "Development of soft gripper for the versatile robot hand," *Mech. Mach. Theory*, vol. 13, no. 3, pp. 351–359, 1978.

[3] A. M. Dollar and R. D. Howe, "The highly adaptive SDM hand: Design and performance evaluation," *Int. J. Robot. Res.*, vol. 29, no. 5, pp. 585–597, 2010.

[4] F. Lotti, P. Tiezzi, G. Vassura, L. Biagiotti, G. Palli, and C. Melchiorri, "Development of UB Hand 3: Early results," in *Proc. IEEE Int. Conf. Robot. Autom.*, Barcelona, Spain, Apr. 2005, pp. 4488–4493.

[5] M. Carrozza *et al.*, "The SPRING hand: Development of a self-adaptive prosthesis for restoring natural grasping," *Auton. Robots*, vol. 16, no. 2, pp. 125–141, Mar. 2004.

[6] A. M. Dollar, L. P. Jentoft, J. H. Gao, and R. D. Howe, "Contact sensing and grasping performance of compliant hands," *Auton. Robots*, vol. 28, no. 1, pp. 65–75, 2010.

[7] J. S. Son, "Integration of tactile sensing and robot hand control," Ph.D. dissertation, Cambridge, MA, USA: Harvard Univ., 1996.

[8] H. Yousef, M. Boukallel, and K. Althoefer, "Tactile sensing for dexterous in hand manipulation in robotics—A review," *Sensors Actuators A: Phys.*, vol. 167, no. 2, pp. 171–187, 2011.

[9] Y. Bekiroglu, J. Laaksonen, J. Jogensen, V. Kyrki, and D. Kragic, "Assessing grasp stability based on learning and haptic data," *IEEE Trans. Robot. Autom.*, vol. 27, no. 3, pp. 616–629, Jun. 2011.

[10] Z. Pezzementi, E. Plaku, C. Reyda, and G. Hager, "Tactile-object recognition from appearance information," *IEEE Trans. Robot. Autom.*, vol. 27, no. 3, pp. 473–487, Jun. 2011.

[11] S. Shirafuji and K. Hosoda, "Detection and prevention of slip using sensors with different properties embedded in elastic artificial skin on the basis of previous experience," in *Proc. Int. Conf. Adv. Robot.*, Tallinn, Estonia, Jun. 2011, pp. 459–464.

[12] F. L. Hammond, R. K. Kramer, W. Qian, R. D. Howe, and R. J. Wood, "Soft tactile sensor arrays for micromanipulation," in *Proc. IEEE/RSJ Int. Conf. Intell. Robots Syst.*, Vilamoura, Portugal, Oct. 2012, pp. 25–32.

[13] M. I. Tiwana, S. J. Redmond, and N. H. Lovell, "A review of tactile sensing technologies with applications in biomedical engineering," *Sens. Actuators A, Phys.*, vol. 179, pp. 17–31, 2012.

[14] B. Belzile and L. Birglen, "A compliant self-adaptive gripper with proprioceptive haptic feedback," *Auton. Robots*, vol. 36, no. 1–2, pp. 79–91, 2014.

[15] G. Carbone, Ed., *Grasping in Robotics*. New York, NY, USA: Springer, 2013.

[16] M. Wassink, R. Carloni, and S. Stramigioli, "Compliance analysis of an under-actuated robotic finger," in *Proc. 3rd IEEE/RAS EMBS Int. Conf. Biomed. Robot. Biomechatronics*, Tokyo, Japan, Sep. 2010, pp. 325–330.

[17] M. Malvezzi and D. Prattichizzo, "Evaluation of grasp stiffness in underactuated compliant hands," in *Proc. IEEE Int. Conf. Robot. Autom.*, Karlsruhe, Germany, May 2013, pp. 2074–2079.

[18] L. U. Odhner *et al.*, "A compliant, underactuated hand for robust manipulation," *Int. J. Robot. Res.*, vol. 33, no. 5, pp. 736–752, Apr. 2014.

[19] B. Belzile and L. Birglen, "Stiffness analysis of double tendon underactuated fingers," in *Proc. IEEE Int. Conf. Robot. Autom.*, Hong Kong, China, May-Jun. 2014, pp. 6679–6684.

[20] M. Kaneko and K. Tanie, "Contact point detection for grasping an unknown object using self-posture changeability," *IEEE Trans. Robot. Autom.*, vol. 10, no. 3, pp. 355–367, Jun. 1994.

[21] M. Huber and R. A. Grupen, "2-d contact detection and localization using proprioceptive information," *IEEE Trans. Robot. Autom.*, vol. 10, no. 1, pp. 23–33, Feb. 1994.

[22] S. Haidacher and G. Hirzinger, "Contact point identification in multi-fingered grasps exploiting kinematic constraints," in *Proc. IEEE Int. Conf. Robot. Autom.*, Washington, D.C., May 2002, vol. 2, pp. 1597–1603.

[23] Y.-L. Park, S. C. Ryu, R. J. Black, K. Chau, B. Moslehi, and M. R. Cutkosky, "Exoskeletal force-sensing end-effectors with embedded optical fiber bragg grating sensors," *IEEE Trans. Robot.*, vol. 25, no. 6, pp. 1319–1331, Dec. 2009.

[24] G. S. Koonjul, G. J. Zeglin, and N. S. Pollard, "Measuring contact points from displacements with a compliant, articulated robot hand," in *Proc. IEEE Int. Conf. Robot. Autom.*, Shanghai, China, May 2011, pp. 489–495.

[25] C. Blanes, M. Mellado, and P. Beltran, "Tactile sensing with accelerometers in prehensile grippers for robots," *Mechatronics*, vol. 33, pp. 1–12, 2016.

[26] L. P. Jentoft and R. D. Howe, "Determining object geometry with compliance and simple sensors," in *Proc. IEEE Int. Conf. Intell. Robots Syst.*, San Francisco, CA, USA, Sep. 2011, pp. 3468–3473.

[27] L. Wang, J. DelPreto, S. Bhattacharyya, J. Weisz, and P. K. Allen, "A highly-underactuated robotic hand with force and joint angle sensors," in *Proc. IEEE/RSJ Int. Conf. Intell. Robots Syst.*, San Francisco, CA, USA Sep. 2011, pp. 1380–1385.

[28] D. Aukes, S. Kimy, P. Garciay, A. Edsinger, and M. R. Cutkosky, "Selectively compliant underactuated hand for mobile manipulation," in *Proc. IEEE Int. Conf. Robot. Autom.*, Saint Paul, MN, USA, May 2012, pp. 2824–2829.

Bruno Belzile received the B.Eng. degree in mechanical engineering from Polytechnique Montréal, Montréal, QC, Canada, in 2011, where he is currently working toward the Ph.D. degree in mechanical engineering in the Robotics Laboratory.

He holds scholarships from the Natural Sciences and Engineering Research Council of Canada (NSERC) and Fonds de recherche du Québec-Nature et technologies (FRQNT).

Lionel Birglen (M'00) received the B.Eng. degree in mechatronics from Ecole Nationale Supérieure des Arts et Industries de Strasbourg, Strasbourg, France, in 2000, and the Ph.D. degree in mechanical engineering from the Robotics Laboratory, Université Laval, QC, Canada.

In 2005, he joined the Department of Mechanical Engineering, Ecole Polytechnique of Montreal, QC, where he is currently a Full Professor in Mechatronics. He is also a member of adjunct faculty with the Department of Electrical Engineering, Université Laval. In 2013, he was a Visiting Associate Professor in the 3ME Department, TU Delft, Delft, The Netherlands. His research interests include the kinematic analysis and control of self-adaptive mechanisms, especially underactuated robotic hands, and with a particular emphasis on force control. He is the author of numerous papers, as well as two books on the topic of underactuated grasping and mechatronics.

Dr. Birglen is a member of the American Society of Mechanical Engineers, the Canadian Committee for the Theory of Machines and Mechanisms, and the Canadian Aeronautics and Space Institute.